Mechanistic Aspect of Reverse Atom Transfer Radical Polymerization of *n*-Butyl Methacrylate in Aqueous Dispersed System

Jian Qiu, Tomislav Pintauer, Scott G. Gaynor, and Krzysztof Matyjaszewski*

Center for Macromolecular Engineering, Department of Chemistry, Carnegie Mellon University, 4400 Fifth Avenue, Pittsburgh, Pennsylvania 15213

Bernadette Charleux and Jean-Pierre Vairon

Laboratoire de Chimie Macromoléculaire, Unité Mixte associée au CNRS, UMR 7610, Université Pierre et Marie Curie, Tour 44, 1er étage, 4, Place Jussieu, 75252 Paris Cedex 05, France

Received April 25, 2000; Revised Manuscript Received August 2, 2000

ABSTRACT: Reverse atom transfer radical polymerization (ATRP) of *n*-butyl methacrylate was conducted in an aqueous dispersed system. Using a water-soluble initiator (V-50), a nonionic surfactant (Brij 98), and a hydrophobic ligand (dNbpy) to complex a copper halide, polymers with relatively well controlled molar masses and low polydispersities were obtained. Stable latexes with particle diameters within 150−300 nm were formed. Kinetic studies were performed under various experimental conditions. The influence of the concentrations of the catalyst, the surfactant, and the initiator as well as the temperature on the polymerization rate, molecular weight, and particle size was investigated. Because of the lack of high molecular weight polymer during the early polymerization stage, reverse ATRP in the aqueous dispersed system presumably has a different "nucleation" mechanism from that of a conventional emulsion polymerization. In addition, fast decomposition of the initiator prevents the continuous entry of radicals into the particles from the aqueous phase. As a result, the kinetics of the reverse ATRP is fundamentally different from a classical emulsion polymerization and is controlled mainly by the atom transfer equilibrium.

Introduction

Polymers with predetermined molar masses and narrow molar mass distribution have traditionally been synthesized only by living ionic and group transfer polymerizations.[1−4] Recent progress in controlled/"living" radical polymerizations (CRP) not only accomplishes the same task but also opens the door to many novel materials with various well-defined compositions and architectures, owing to a larger range of monomers available for radical than for ionic polymerizations.[5,6] Furthermore, radical polymerizations can be conducted under less strict conditions and are more tolerant to protic impurities such as water, which allows the widely employed polymerizations in aqueous dispersed systems, including emulsion, suspension, dispersion, etc.[7−9] With more and more demand for both environmentally friendly manufacturing processes and precise polymer synthesis, it can certainly be predicted that a combination of the established technologies in aqueous dispersed systems with the CRP methods would have a tremendous impact on the future development of the polymer industry.

During the past 2 years, several attempts at applying the existing controlled radical polymerization techniques to the aqueous dispersed systems were reported. The methods employed include stable free radical polymerization (SFRP),[10−13] atom transfer radical polymerization (ATRP),[14−18] reversible addition−fragmentation chain transfer (RAFT),[19,20] and degenerative transfer polymerization based on the iodine atom exchange.[21,22] For SFRP using TEMPO derivatives, only the (co)polymerization of styrene (and derivatives) was successful when conducted above 120 °C and under pressure.[23−25] Recently, a more versatile and bulkier nitroxide, *N*-*tert*-butyl-*N*-(1-diethylphosphono-2,2-dimethylpropyl) nitroxide (SG1), was used to reduce the emulsion polymerization temperature to 90 °C.[26,27] Compared with SFRP, the RAFT technique is more adaptable to the aqueous dispersed system. Relatively well controlled poly(meth)acrylates, polystyrene, and several block copolymers were obtained in emulsion and miniemulsion systems using dithioesters or xanthates derivatives as the chain transfer agents.[19,20,28,29] However, to date, few studies on the kinetics and latex properties are available. Degenerative transfer polymerization of styrene via iodine exchange was also reported in emulsion and miniemulsion.[30−32] As proof for the "living" character, a linear relationship between the molar mass and the monomer conversion was obtained under a carefully designed experimental protocol. The inherent limitation of this system, however, is the small transfer constant of the iodine compound. As a result, the obtained polymers usually have high polydispersities ($M_w/M_n > 1.5$).

Although most transition metal complexes decompose rapidly in water, the Pd, Ru, and Cu complexes that catalyze ATRP are fortunately quite stable. With ruthenium[33] and palladium[34] catalytic systems, a relatively well controlled polymerization of methyl methacrylate was achieved in aqueous systems with or without surfactant. The copper-mediated water-borne ATRP is so far the most versatile system. It has been successfully employed for the (co)polymerization of styrene, acrylates, and methacrylates.[35−39] The polymerization can start either with an alkyl halide and a Cu^I complex[40] or with a conventional radical initiator and a Cu^{II} complex.[41] The latter process is called the reverse ATRP. The current work is a continuation of our prior reverse ATRP studies and addresses mechanistic issues such as the parameters affecting the polymerization

10.1021/ma000720q CCC: $19.00
Published on Web 09/14/2000

Table 1. Typical Reverse ATRP Recipe

component		amount	
monomer	*n*-BMA	3.7 g or 4.1 mL	400 equiv
water		25 g	monomer/water = 15/100 (w/w)
initiator	V-50	17.7 mg	1 equiv
catalyst	$CuBr_2$	21.8 mg	1.5 equiv
ligand	dNbpy	79.6 mg	3 equiv
surfactant	Brij 98	0.5 g	13.5 w % vs monomer
temp	90 °C		

rate, the molecular weight control, the particle size, etc. Efforts were also made toward a better understanding of the similarities and differences between reverse ATRP, conventional emulsion, and miniemulsion polymerizations.

Experimental Section

Materials. *n*-Butyl methacrylate was distilled under reduced pressure after being washed with a 10% aqueous sodium hydroxide solution. 2,2′-Azobis(2-methylpropionamidine) dihydrochloride (V-50) was obtained from Wako and recrystallized from cold methanol/water. Dimethylbipyridine (dMbpy) was purified by recrystallization from ethanol. Diisopropylamine was distilled from CaH_2 and stored under N_2 over molecular sieves. Unless specified, all other reagents were purchased from commercial sources and used without further purification.

4,4′-Di(5-nonyl)-4,4′-bipyridine (dNbpy). dNbpy was synthesized according to a modified literature procedure.[42] A dry 1000 mL round-bottom flask equipped with a magnetic stir bar was put under nitrogen at −78 °C, followed by the addition of 250 mL of dry THF and 48 mL of dry diisopropylamine (0.34 mol) via syringes. A 150 mL aliquot of *n*-BuLi (2.5 M in hexane, 375 mmol) was added to the flask dropwise via cannula. After the mixture was stirred at −78 °C for 2 h, 14.7 g of dMbpy (80 mmol) dissolved in 400 mL of dry THF was then added slowly to the flask via cannula. The mixture turned dark brown immediately. Two hours later, 51.5 mL of bromooctane (0.48 mol) was added quickly via syringe. The reaction mixture was allowed to warm to room temperature overnight. The brown-green solution was then poured into 1000 mL of cold brine. The aqueous phase was extracted with 3 × 100 mL of ethyl acetate. The combined organic phases (light yellow) were dried over $MgSO_4$. After the solvent was removed, the orange viscous residue was Kugelrohr distilled at 170−175 °C/3.5×10^{-2} Torr. A 31 g yield of product was obtained, which slowly crystallized in the freezer (95% yield). ^{1}H NMR (300 MHz, $CDCl_3$) δ (ppm): 0.85 (t, 12H), 1.25 (m, 16H), 1.68 (m, 8H), 2.63 (m, 2H), 7.13 (d, 2H), 8.28 (s, 2H), 8.59 (d, 2H).

Polymerization Recipe and Procedure. Table 1 lists the typical recipe used for reverse ATRP. When necessary, changes were made to the amount of the initiator, the catalyst, the surfactant, and the temperature to investigate the influence of these factors on the polymerization.

An example of the polymerization procedure follows: Brij 98 (0.5 g) and a magnetic stir bar were added to a 50 mL Schlenk flask. The flask was then sealed with a glass stopper and deoxygenated by applying vacuum and backfilling with nitrogen. A 24 mL aliquot of deionized water (previously purged with nitrogen) was added through the sidearm via syringe. The mixture was stirred until the surfactant dissolved. In a separate round-bottom flask, a solution of $CuBr_2$ (21.8 mg) and dNbpy (79.6 mg) in 4.1 mL of BMA was prepared under nitrogen and then cannula transferred to the Schlenk flask. After an emulsion formed under stirring, the Schlenk flask was placed in an oil bath set at 90 °C. A 1 mL aliquot of the aqueous initiator solution (17.7 mg/mL) was finally added, which corresponds to the time zero point for the polymerization. The magnetic stirring rate was kept at 500 rpm. Samples were withdrawn periodically via syringe to monitor the conversion, the molecular weight, and the particle size.

The polymerization was also carried out in a 50 mL three-neck round-bottom flask equipped with a nitrogen inlet and a condenser connected to a bubbler. The procedure was similar to that described above, except that the emulsion was prepared in air, followed by nitrogen bubbling for at least 1 h before the initiator was added. Throughout the polymerization, a small nitrogen flow was maintained. The drawback of this experimental setup, however, is the monomer loss through evaporation. This affects the accuracy of the conversion measurement, especially for a small-scale reaction with a slow polymerization rate.

Characterization. The monomer conversion was measured by both gas chromatography (GC) and gravimetric methods. A portion of the latex sample was dissolved in THF and injected directly into a Shimadzu GC-14A gas chromatograph. Conversions were obtained from the residual monomer content in the samples. Another portion of the samples was dried in an oven at 70 °C. The conversion was calculated from the percentage of the recovered polymer. For all the experiments reported in this paper, the conversion data from both methods agree very well, indicating a negligible amount of monomer evaporation during the polymerization. The solid recovered from gravimetry was dissolved in THF and passed through a small alumina column to remove the catalyst. After being filtered through a 0.2 μm syringe filter, the obtained colorless solution was injected onto SEC columns (Polymer Standard Service 10^5, 10^3, and 100 Å and guard, Waters 717plus autosampler). A calibration curve based on linear poly(methyl methacrylate) standards was used in conjunction with a differential refractometer to determine the molecular weights and polydispersities.

Particle diameters were measured by dynamic light scattering (Zetasizer4 from Malvern or ZetaPlus from Brookhaven). The latex samples were diluted with an aqueous 10 mM KCl solution before the measurement.

Partitioning Experiments. Solutions of CuBr (or $CuBr_2$)/dNbpy(1/2 ratio) in BMA were prepared at various concentrations. The solutions were mixed with deionized water in a 15/100 (w/w) ratio. The biphasic mixture was stirred at room temperature or at 90 °C for at least 1 h. (The absorption of the organic phase did not change with longer stirring time, indicating the partition equilibrium was reached.) The two phases were then separated and measured on a UV/vis/NIR spectrometer (Lambda 900, Perkin-Elmer). In the case of CuBr/2dNbpy, the experiment was performed under nitrogen. The concentrations of the Cu^I and Cu^{II} complexes in the organic phase were calculated from the absorbances at 460 and 742 nm, respectively. For comparison, the concentration of Cu^{II} in the aqueous phase was also determined. In a typical experiment, an excess of the strongly binding ligand tris(2-(dimethylamino)ethyl)amine (Me_6TREN) was added to the aqueous phase after separation, and the concentration of Cu^{II} was calculated on the basis of the complex absorbance at 880 nm.

The partitioning of dNbpy in the presence of $CuBr_2$ was determined gravimetrically. The organic phase was evaporated after separation, and the amount of dNbpy was calculated by extracting the amount of $CuBr_2$ from the solid content. The former was based on the results from the UV measurement. The partitioning of dNbpy alone between the two phases was obtained in a similar way, except that the concentration of dNbpy in the organic phase was measured by reverse phase high-performance liquid chromatography (HPLC). HPLC was performed using a Shimadzu LC 10AD pump, 712 WISP autosampler, Waters Nova-Pak C18 column (3.9 × 150 mm), Waters 486 tunable absorbance detector, and 410 differential refractometer at 35 °C with acetonitrile as the eluent.

Partitioning of the surfactant was also measured by the gravimetric method. Solutions of Brij 98 in deionized water were prepared at different concentrations. The solutions were mixed with BMA in a 100/15 (w/w) ratio. The mixture was stirred at room temperature or 90 °C overnight. The stirring was then stopped, and the emulsion was kept at the same temperature until phase separation occurred. From the solid

Table 2. Partitioning of $CuBr_2$/2dNbpy and CuBr/2dNbpy in BMA and Water;[a] BMA/Water (w/w) = 15/100

		$CuBr_2$/2dNbpy						CuBr/2dNbpy		
initial concn[b]		2.5×10^{-2} M		1.0×10^{-2} M		2.5×10^{-3} M		3.0×10^{-2} M	2.5×10^{-2} M	1.0×10^{-2} M
λ	r.t.	11.9	8.1[c]	1.6	4.4[c]	0.2	0.3[c]	71	160	160
λ	90 °C	0.4	1.5[c]	0.2	0.4[c]	*d*	0.1[c]	13	21	19
$[Cu]_{org}/[Cu]_{init}$	r.t.	64%	55%[c]	24%	40%[c]	3%	4%[c]	91%	96%	96%
$[Cu]_{org}/[Cu]_{init}$	90 °C	12%	18%[c]	3%	5%[c]	*d*	1%[c]	66%	76%	74%

[a] Unless noted, the concentrations of the Cu^{II} and Cu^{I} complex were measured in the organic phase based on the absorbance at 742 nm (ϵ = 230 L mol^{-1} cm^{-1}) and 460 nm (ϵ varies with concentration), respectively. [b] The concentration in the organic phase before mixing with water. [c] The concentration of Cu^{II} in the organic phase was calculated based on the measurement of Cu^{II} in the aqueous phase by complexation with Me_6TREN (λ_{MAX} = 880 nm, ϵ = 400 L mol^{-1} cm^{-1}). [d] The signal in the organic phase is too small to detect.

content recovered from the aqueous phase, the concentration of the surfactant in water was obtained.

The critical micellar concentration (cmc) of Brij 98 was determined through surface tension measurements, using the Du Nouy Ring method (Cenco model 70545).

Results and Discussion

The key to a controlled radical polymerization is to maintain a fast equilibrium between the growing radicals and the dormant species. In ATRP or reverse ATRP, such an equilibrium is achieved by using a metal complex that switches between n and $n + 1$ oxidation states (eq 1).

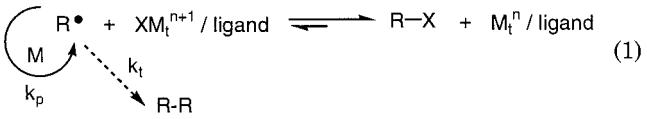

(1)

The same principle holds for aqueous dispersed systems. Since the polymer chains grow in the organic phase, the first requirement for control over the polymerization is to have sufficient concentrations of both the activator (metal complex at the lower oxidation state) and the deactivator (metal complex at the higher oxidation state) in the organic phase. Otherwise, either no polymerization or an uncontrolled polymerization would occur. Therefore, the choice of the proper ligand becomes crucial. In our previous studies,[40] a successful polymerization was only achieved when ligands that displayed sufficient hydrophobicity were employed, such as 4,4′-di(5-nonyl)-2,2′-bipyridine (dNbpy), 4,4′-dialkyl-2,2′-bipyridine (dAbpy, alkyl: mixture of *n*-pentyl and 5-nonyl), or *N*,*N*-bis(2-pyridylmethyl)octadecylamine (BPMODA). On the other hand, ligands such as 2,2′-bipyridine (bpy), *N*,*N*,*N*′,*N*″,*N*″-pentamethyldiethylenetriamine (PMDETA), or tris[2-(dimethylamino)ethyl]-amine (Me_6TREN) that function very well in bulk or solution polymerizations led to uncontrolled polymerizations in aqueous dispersed systems. We ascribed this outcome to the different partitioning behavior of the metal complexes. To better understand the catalyst performance in the heterogeneous system, we measured the partitioning of both CuBr/dNbpy and $CuBr_2$/dNbpy (the ratio of Cu/ligand was kept as 1/2) between *n*-BMA and water.

Partitioning of the Metal Complexes. Copper complexes display characteristic absorption in the UV−vis region; therefore, UV−vis spectroscopy was applied to measure the partitioning of the complexes between *n*-BMA and water, as described in the Experimental Section. Shown in Table 2 are the results from the partitioning studies. The apparent partitioning coefficient (λ) is defined as $\lambda = [Cu]_{org}/[Cu]_{aq}$.

λ depends on the total concentration of Cu^{II}/2dNbpy as well as on the temperature. The higher the amount of Cu^{II}/2dNbpy used or the lower the temperature, the larger the percentage of the Cu^{II} species that remains in the organic phase. A comparison of the absorption spectra of the Cu^{II} in the organic phase before and after mixing with water (Figure 1) reveals a remarkable change of the relative intensity of the peaks around 530 and 740 nm. The former absorbance most likely comes from $CuBr_3^-$ or $CuBr_4^{2-}$ anions, as suggested in the literature,[43−45] while the latter is from the trigonal-bipyramidal complex $[Cu(dNbpy)_2Br]^+$.[46] A reasonable explanation for the decrease in the 530 nm band absorbance is that $CuBr_3^-$ or $CuBr_4^{2-}$ dissociates into $CuBr_2$ and Br^- upon contact with water. $CuBr_2$ is highly soluble in water (its solubility at 25 °C is 126 g in 100 g of water[47]) and therefore migrates easily to the aqueous phase. At higher temperatures, the equilibrium between $CuBr_3^-$ (or $CuBr_4^{2-}$) and $[Cu(dNbpy)_2Br]^+$ shifts toward the former species,[46] enhancing the aqueous partitioning of the Cu^{II} species and leaving more free dNbpy in the organic phase. This explains the temperature dependence of the partitioning behavior.

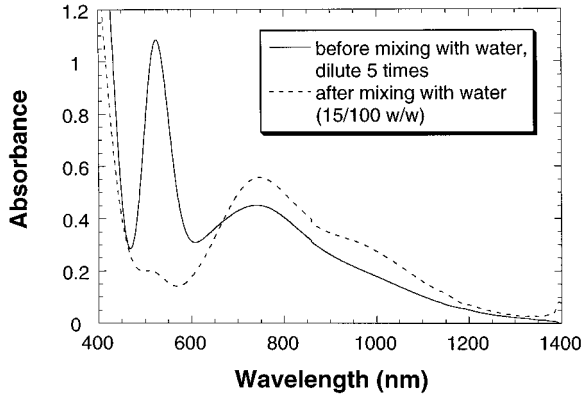

Figure 1. Absorption spectra of $CuBr_2$/2dNbpy in *n*-BMA at room temperature before and after mixing with water. Initial concentration of $CuBr_2$/dNbpy: 1.0×10^{-2} M. *n*-BMA/water = 15/100 (w/w).

This anion dissociation, however, is not the only cause for the aqueous partitioning of Cu^{II}, because even for a $Cu(CF_3SO_3)_2$/2dNbpy complex where no copper-based anion is present, there is still a significant amount of Cu^{II} in the aqueous phase, as shown in Table 3. dNbpy is quite hydrophobic, and the aqueous partitioning of dNbpy alone is negligible according to the HPLC measurements. In the presence of Cu^{II}, some dNbpy enters the aqueous phase in the form of a complex with Cu^{II}, but its concentration is much lower than that of the total Cu^{II} in water. This suggests that the coordination between Cu^{II} and dNbpy is reversible to a certain extent; i.e., the complex $[Cu(dNbpy)_2Br]^+$ partially dissociates and releases Cu^{2+}, which is preferentially soluble in the aqueous phase, and the majority of free dNbpy and the remaining $[Cu(dNbpy)_2Br]^+$ stay in the

Scheme 1. Partitioning of $CuBr_2$/2dNbpy between the Nonpolar Organic Phase and the Aqueous Phase

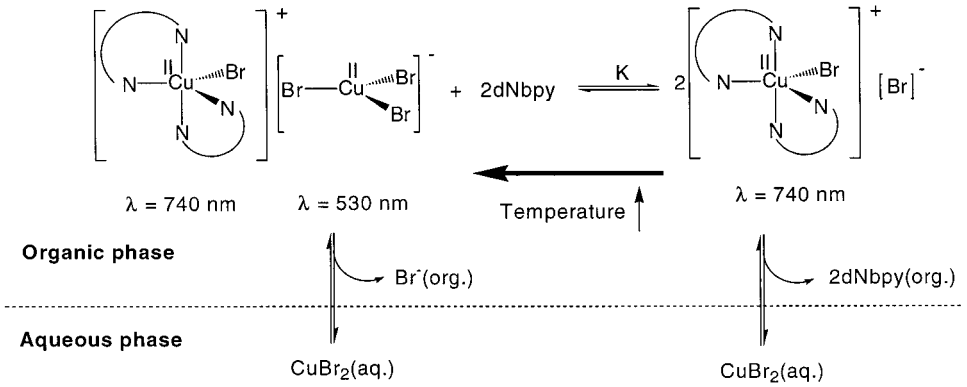

Table 3. Comparison of the Partitioning of $CuBr_2$/2dNbpy and $Cu(CF_3SO_3)_2$/2dNbpy in the Organic Phase (in %);[a] BMA/Water (w/w) = 15/100

initial concn (M)[b]		2.5×10^{-2}	1.0×10^{-2}	2.5×10^{-3}
Cu^{II} from $CuBr_2$/2dNbpy	r. t.	55	40	4
	90 °C	18	5	1
Cu^{II} from $Cu(CF_3SO_3)_2$/2dNbpy	r.t.	78	71	61
	90 °C	55	59	49
dNbpy from $CuBr_2$/2dNbpy	r.t.	85	91	94
	90 °C	69	79	80
dNbpy from $Cu(CF_3SO_3)_2$/2dNbpy	r.t.	94	100	100
	90 °C	67	83	85

[a] The partitioning of Cu^{II} in the organic phase was calculated based on the measurement of Cu^{II} in the aqueous phase by complexation with Me_6TREN (λ_{MAX} = 880 nm, ϵ = 400 L mol^{-1} cm^{-1}). [b] Initial concentration of the complex in BMA before mixing with water.

organic phase. At lower concentrations of $CuBr_2$/2dNbpy in the organic phase, the ratio of dNbpy to water is decreased, and water can then compete with dNbpy more successfully and extract the cupric cation to the aqueous phase. This explains the concentration dependence of the apparent partitioning coefficient λ, which takes all different Cu^{II} species into account.

Scheme 1 summarizes the partitioning of the $CuBr_2$/2dNbpy complex between the organic phase and the aqueous phase. As a consequence of the equilibrium shift between different coexisting Cu^{II} species, the absorption spectrum of the organic phase changes dramatically. Accompanying this is a variation in the $CuBr_2$ to dNbpy ratio in the organic phase after mixing with water. To prove this speculation, we recorded the spectra of Cu^{II} complex at different ratios of dNbpy to $CuBr_2$ in pure BMA (Figure 2). When the ratio dNbpy/$CuBr_2$ increases, the absorption at 530 nm progressively decreases until it totally disappears, while the absorption at 742 nm is relatively unaffected. This phenomenon resembles what was observed in Figure 1 for the spectrum after mixing with water. Therefore, in the presence of water, the ratio of dNbpy to $CuBr_2$ in the organic phase is much larger than the initial ratio 2 to 1, and free dNbpy is in excess. The concentration of copper species remaining in the organic phase is estimated from the absorbance at 742 nm, using the extinction coefficient of $CuBr_2$/2dNbpy (ϵ = 230 L mol^{-1} cm^{-1}), since the absorption at this wavelength is nearly independent of the ratio of $CuBr_2$ to dNbpy (Figure 2). More accurate values can be obtained by analyzing the corresponding aqueous phase after complexation with Me_6TREN. Me_6TREN is a very strongly coordinating

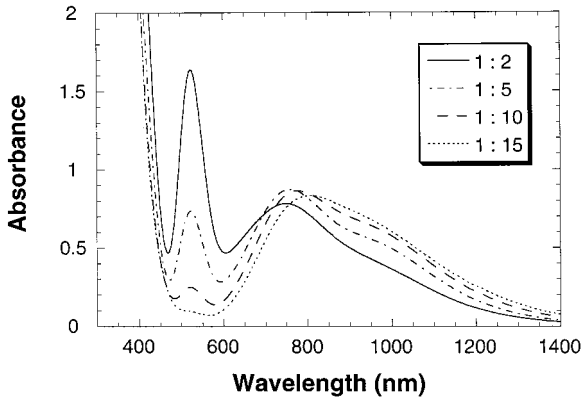

Figure 2. Absorption spectra of $CuBr_2$/dNbpy in *n*-BMA at room temperature with different ratio of $CuBr_2$ to dNbpy. Concentration of $CuBr_2$: 3×10^{-3} M.

ligand (binding constant to Cu^{II} in H_2O is approximately 10^{15}),[48] and the extinction coefficient of the corresponding 1:1 complex at 880 nm is 400 L mol^{-1} cm^{-1}, which provides reasonable accuracy in the experiments carried out. As shown in Table 2, the results obtained from both phases agree quite well.

Compared with the Cu^{II} species, the Cu^{I} complex is much more soluble in the organic phase. The partitioning is little influenced by the concentration but is dependent on temperature. At 90 °C, about 20−30% of the initial Cu^{I} is dissolved in the aqueous phase (most likely in the form of $[CuBr_2]^-$),[49] which allows for a certain degree of catalyst transportation through the aqueous phase.

It should be noted that the partitioning studies were performed in the absence of the surfactant. It is possible that the values of the partition coefficient may change in systems where surfactant is involved. Nevertheless, we anticipate that the above results still provide valuable estimates of the partitioning behavior of the metal complexes in those cases. They suggest that dNbpy is not the ideal ligand to keep most of the copper species in the organic phase. Yet, it still affords reasonable control over the polymerization in the aqueous dispersed systems. While the search for more efficient ligands continues, we report our current results based on the experiments using dNbpy as the ligand.

Polymerization. The typical reverse ATRP was conducted under the conditions described in Table 1. Meanwhile, other experimental variations were also applied to better understand the mechanistic aspects of the polymerization. These recipes are summarized in Table 4. The variables include the amount of the

Table 4. Experimental Conditions for Reverse ATRP in Aqueous Dispersed Systems

exp	temp (°C)	Brij 98 (wt % vs BMA)	H_2O (mL)	BMA (mL)	V-50 (mg)	$CuBr_2$ (mg)	dNbpy (mg)	M/I/$CuBr_2$/dNbpy
1	90	0.5 g (13.5%)	25	4.1	17.7	21.8	79.6	400/1/1.5/3
2	90	0.18 g (13.5%)	10	1.5	6.4	0	0	400/1/0/0
3[a]	90	0.18 g (13.5%)	10	1.5	6.4	0	28.9	400/1/0/3
4[b]	90	0.5 g (13.5%)	10	1.5	6.4	7.9	0	400/1/1.5/0
5	90	0.5 g (13.5%)	25	4.1	17.7	14.6	53.3	400/1/1/2
6	90	0.19 g (5.0%)	25	4.1	17.7	21.8	79.6	400/1/1.5/3
7[c]	90	0.74 g (5.0%)	100	16.6	70.8	58.4	213.2	400/1/1/2
8	90	0.10 g (2.7%)	25	4.1	17.7	21.8	79.6	400/1/1.5/3
9	90	0.18 g (13.5%)	10	1.5	12.8	15.8	58.0	200/1/1.5/3
10	80	0.5 g (13.5%)	25	4.1	17.7	14.6	53.3	400/1/1/2

[a] dNbpy was dissolved in BMA. [b] $CuBr_2$ was dissolved in the aqueous phase together with Brij 98 before the addition of BMA. [c] Reaction was carried out in a 250 mL conventional thermostated reactor with mechanical stirring at 400 rpm.

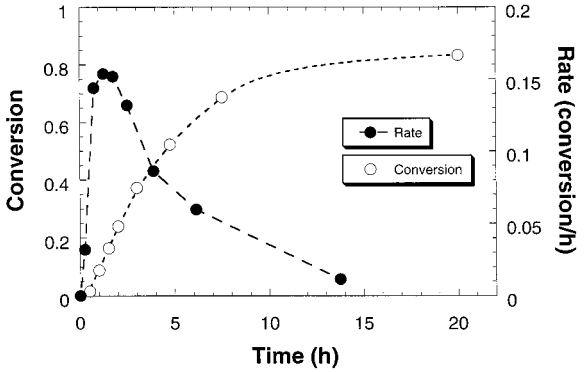

Figure 3. Kinetics of *n*-BMA under typical reverse ATRP conditions (Table 1 and experiment 1 in Table 4).

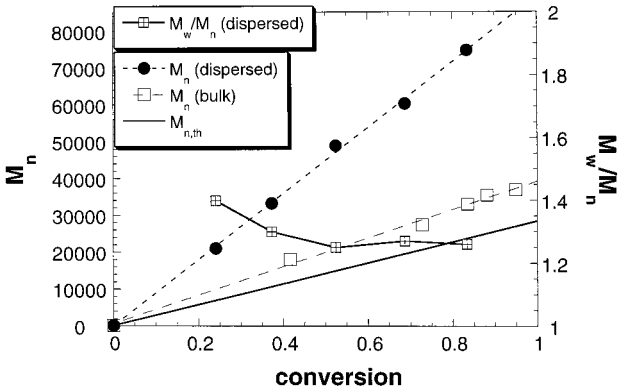

Figure 4. Dependence of molecular weight and polydispersity on monomer conversion for the typical reverse ATRP in aqueous dispersed system and in bulk. *n*-BMA/initiator/$CuBr_2$/dNbpy = 400/1/1.5/3, 90 °C. Bulk: AIBN as the initiator. Aqueous dispersed system: V-50 as the initiator, *n*-BMA/water = 1.5/10 (w/w), 13.5 w% of Brij 98 vs monomer (experiment 1 in Table 3).

catalyst (entry 2,3,4/1,5/6,7), the surfactant (entry 1,6,8/5,7), the initiator (entry 9), and the temperature (entry 10).

1. Typical Reverse ATRP. Figure 3 shows the conversion and the polymerization rate curves for a typical reverse ATRP in the aqueous dispersed system (exp.1). Because of the limited number of experimental data points, a precise polymerization rate curve is not available. The current curve is obtained by plotting $[\mathrm{conv}(t_n) - \mathrm{conv}(t_{n-1})]/(t_n - t_{n-1})$ against $^1/_2(t_n + t_{n-1})$ and serves only for the purpose of a qualitative kinetic analysis.

During the first 30−45 min, there was little to no conversion. However, the color of the emulsion gradually turned from light green to light brown during this induction period. Green is the characteristic color of $CuBr_2$/dNbpy complex in the organic phase, while brown is the color for CuBr/dNbpy complex. This color change indicates that, prior to the polymerization, the initial Cu^{II} is nearly completely replaced by Cu^{I} after reaction with the radicals. Following the induction period, the polymerization rate increases rapidly and reaches the maximum around 10−30% monomer conversion. Thereafter until complete conversion, the polymerization rate decreases, characterizing the last stage of the polymerization.

Two important features of controlled radical polymerizations are observed in the typical reverse ATRP in the aqueous dispersed system. The first one is the linear increase of molecular weights with monomer conversion, as shown in Figure 4, indicating that the number of chains is constant. In other words, chain transfer reactions are negligible. The second feature is the low polydispersities of the polymer chains (<1.5), meaning that nearly all the chains start to grow simultaneously.

Compared with the bulk reverse ATRP carried out under similar conditions,[50] the drawback of the aqueous dispersed system is the relatively low initiation efficiency (around 30%, versus 70% for the homogeneous system, Figure 4), calculated on the basis of the theoretical molecular weight values, assuming that one molecule of initiator generates two radicals (initiation efficiency $f = M_{n,th}/M_n = M_0 \times ([M]_0/2[I]_0) \times \mathrm{conv}/M_n$, M_0 is the molar mass of the monomer). Such a low efficiency is mainly attributed to the radical termination in the aqueous phase, which might include the reaction between two radicals or between radicals and $CuBr_2$ dissolved in water. The latter is a known radical inhibitor.[51]

The final latex is usually very stable, lasting from days to even more than a year without any sedimentation. The particle size is quite reproducible, on the average of 195 ± 10 nm for six separate experiments under identical conditions.

2. Effect of the Deactivator Concentration. Both $CuBr_2$ and dNbpy are essential to achieve a controlled polymerization. This is demonstrated by the results shown in Table 5, where three reactions were carried out under conditions similar to experiment 1 in Table 4, except that either $CuBr_2$ (experiment 3) or dNbpy (experiment 4) or both (experiment 2) were absent. None of these polymerizations are controlled, as expected. The presence of $CuBr_2$ in the aqueous phase decreases the polymerization rate slightly; however, the induction periods in all three experiments are negligible compared with that observed in the typical reverse ATRP (experiment 1). This suggests that the latter induction period is the outcome of the deactivation process in the organic phase. The particle size is unaffected by the presence

Table 5. Polymerizations in the Absence of $CuBr_2$ and/Or DNbpy[a]

exp.	I/$CuBr_2$/dNbpy	time (min)	conv (%)	$M_{n,th}$	$M_{n,sec}$	M_w/M_n	PS (nm)
2	1/0/0	5	49	13 940	73 920	3.89	
		10	87	24 740	110 000	3.00	
		15	98	27 870	105 600	3.20	117
3	1/0/3	5	49	13 940	114 800	3.09	
		10	97	27 590	139 400	2.74	
		15	98	27 870	138 900	2.81	116
4	1/1.5/0	5	29	8 250	98 380	2.57	
		10	73	20 760	99 410	2.80	
		15	95	27 020	97 750	2.87	143

[a] See Table 4 for experiment conditions.

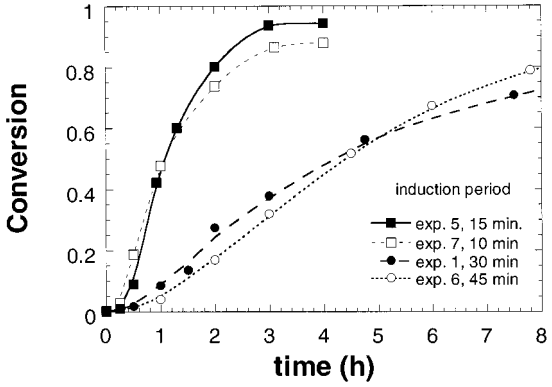

Figure 5. Kinetics of *n*-BMA with different amount of catalyst and surfactant (see Table 4 for experimental conditions). Experiment 5: $[CuBr_2/2dNbpy]_0/[V\text{-}50]_0 = 1.0$, Brij 98 = 13.5%. Experiment 7: $[CuBr_2/2dNbpy]_0/[V\text{-}50]_0 = 1.0$, Brij 98 = 5%. Experiment 1: $[CuBr_2/2dNbpy]_0/[V\text{-}50]_0 = 1.5$, Brij 98 = 13.5%. Experiment 6: $[CuBr_2/2dNbpy]_0/[V\text{-}50]_0 = 1.5$, Brij 98 = 5%.

of dNbpy but is larger in the presence of aqueous $CuBr_2$, probably due to the rise in the ionic strength of the water phase, which modifies the partitioning of Brij98 between the aqueous and the organic phases.[52]

In the presence of both $CuBr_2$ and dNbpy, the initial ratio of $CuBr_2$/2dNbpy to the initiator has a great effect on the kinetics of reverse ATRP. The comparison of experiments 1 and 5 or experiments 6 and 7 (Table 4) shows that the polymerization is much faster when less $CuBr_2$/2dNbpy is employed (Figure 5). In fact, when the concentration of $CuBr_2$/2dNbpy is decreased from 1.5 to 1.0 equiv with respect to the initiator, the maximum polymerization rate increases by a factor of 4−5 instead of 1.5. This can be ascribed to different amount of the deactivator remaining after the deactivation reaction, as well as to the concentration dependent partitioning of Cu^{II} species, as shown in Table 2.

Shown in Figure 6 are the comparisons of the molar mass evolution with different ratios of $CuBr_2$/2dNbpy vs the initiator at two surfactant concentrations. With more $CuBr_2$/2dNbpy, the polydispersity of the obtained polymer is slightly lower. This is related to slower propagation and agrees with the higher partitioning of the deactivator in the organic phase, thus affording more efficient deactivation. In contrast, the evolution of the molar mass of the polymers is not sensitive to the amount of the deactivator. As mentioned earlier, the initiation efficiency is affected mainly by the radical termination in the aqueous phase. The approximate independence of the initiation efficiency on the initial amount of the copper complex indicates that the $CuBr_2$ dissolved in water (the amount increases with the total Cu^{II} concentration) is not the major cause for the irreversible termination in the aqueous phase. Rather, the termination between two radicals is the factor determining the initiation efficiency.

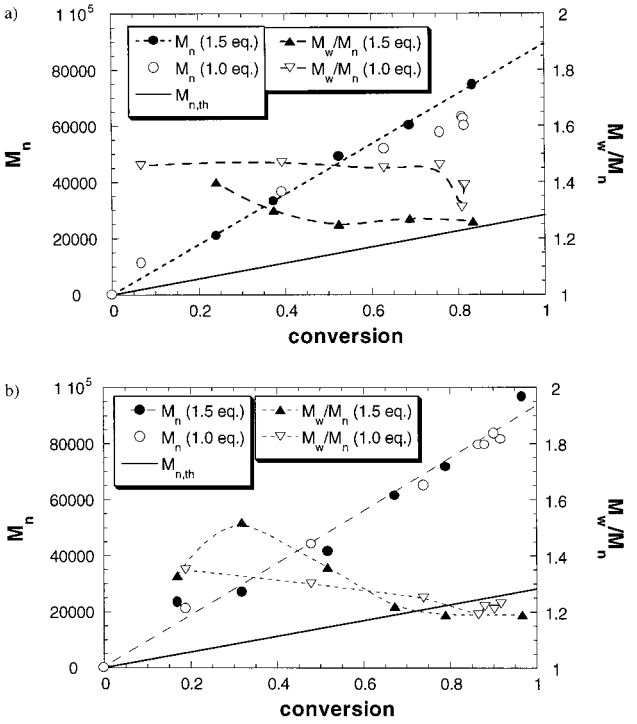

Figure 6. Effect of the amount of initial $CuBr_2$/2dNbpy on the molecular weight evolution. The values in the bracket represent the molar ratio of $[CuBr_2/2dNbpy]_0$ to $[V\text{-}50]_0$. (a) 13.5 wt % of Brij 98.

Table 6. Final Particle Size with Different Amounts of Brij 98 and $CuBr_2$/2dNbpy

		$CuBr_2$/2dNbpy vs V-50	
		1.0 equiv	1.5 equiv
Brij 98	5.0%	215 nm[a]	236 ± 18 nm[b]
vs BMA	13.5%	189 ± 5 nm[c]	195 ± 10 nm[d]

[a] Value from one experiment (92% conversion). [b] Average value from three separate experiments (90−97% conversion). [c] Average value from two separate experiments (82−94% conversion). [d] Average value from six separate experiments (91−98% conversion).

The particle size is quite sensitive to the amount of the metal complex, as shown in Table 6. The variation in the particle diameters with the amount of the catalyst is more pronounced at lower levels of the surfactant. This probably results from the different ionic strength of the aqueous phase. With more $CuBr_2$ dissolved in the aqueous phase, the increasing ionic strength may change the partitioning of the surfactant and enhance the rate of particle coalescence, leading to a latex with a larger average particle size.

3. Effect of the Amount of the Surfactant. Neither the polymerization rate (compare experiments 1 and 6 or experiments 5 and 7 in Figure 5) nor the molecular

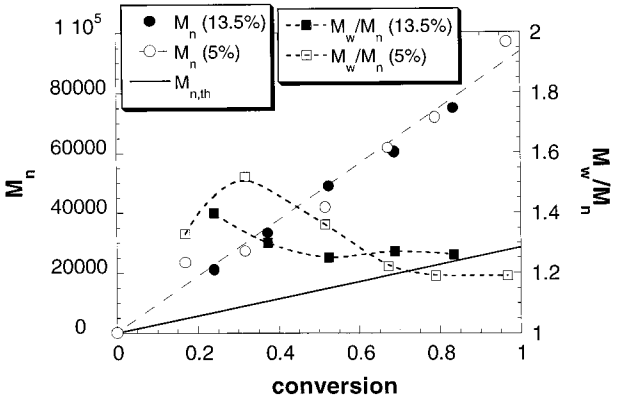

Figure 7. Effect of the amount of Brij 98 on the molecular weight evolution. $CuBr_2$/2dNbpy = 1.5 equiv. The values in the bracket represent the weight percentage of the surfactant against the monomer (see Table 4 for experimental conditions).

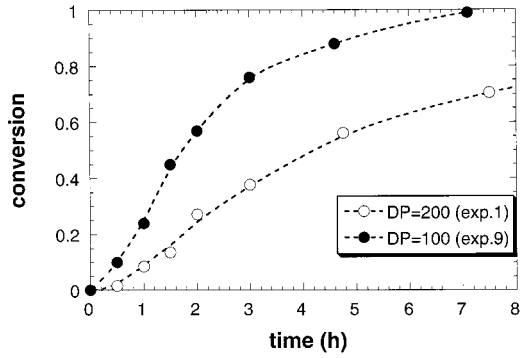

Figure 8. Kinetics of *n*-BMA with different amount of initiator (see Table 4 for experimental conditions).

weight (Figure 7) is affected much by the amount of the surfactant used. On the contrary, the final particle size and the latex stability are very dependent on the quantity of the surfactant, as we have already seen in Table 6. With 2.7 w% of Brij 98 (vs monomer, experiment 8), serious coagulation occurred. With 5% of the surfactant, the latex was much more stable, although some coagulum was still observed on the stir bar and the wall of the reaction flask (about 10% vs the solid content at 97% conversion). When the surfactant was increased to 13.5%, the emulsion was very stable, no coagulum was observed, and smaller particle diameters were obtained.

The conclusions from the above results are as follows: first, the surfactant Brij 98 does not interfere with the atom transfer reaction, nor does it act as a chain transfer agent; second, the particle size, and hence the number of particles, has little effect on the polymerization rate. The latter observation is very different from the kinetics of conventional emulsion and miniemulsion polymerizations and will be discussed further later.

4. Effect of the Initiator Concentration. The higher the concentration of the initiator, the larger the number of growing chains and therefore the faster the rate of the polymerization should be. On the other hand, radical termination occurs more rapidly as well, leading to a decreased initiator efficiency and consequently to the formation of a larger excess of Cu^{II} species. The two phenomena have opposite effects on the polymerization rate, which depends on the ratio $[Cu^{I}][\text{growing chains}]/[Cu^{II}]$. Shown in Figure 8 are the kinetic results from two experiments targeting a DP of 100 (experiment 9) or 200 (experiment 1). The faster polymerization rate

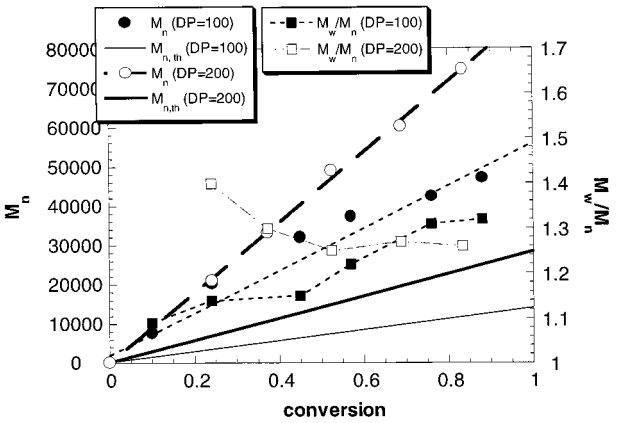

Figure 9. Effect of the amount of initiator on the molecular weight evolution (see Table 4 for experimental conditions).

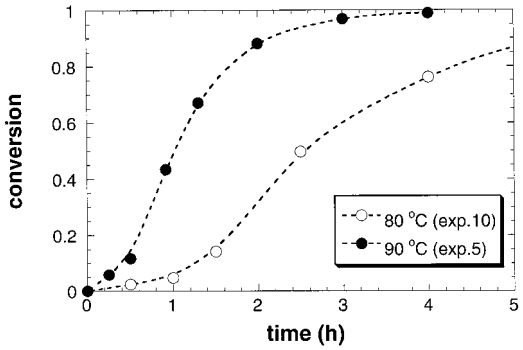

Figure 10. Kinetics of *n*-BMA at different temperature (see Table 4 for experimental conditions).

observed in experiment 9 indicates that the propagating radicals are still greater in number despite the enhanced termination rate. The molecular weight and polydispersity evolutions are given in Figure 9. The slight curvature of the molecular weight development and the increasing polydispersity for DP = 100 suggests a considerable amount of a chain transfer process, the cause of which is still unclear. This result, however, does not imply that polymers with lower target molecular weights cannot be well controlled in the aqueous dispersed system. Like in bulk or solution ATRP, reaction conditions need to be adjusted accordingly to suit different experimental purposes.

The final particle size for DP = 100 (273 nm) is about 70 nm larger than that of DP = 200. In classical emulsion polymerization, the particle diameter usually decreases as the concentration of the initiator increases. However, under the experimental condition of experiment 9, the initial concentration of $CuBr_2$ was also doubled, which may be responsible for the enlarged particle size, as discussed earlier.

5. Effect of Temperature. The decomposition rate of the initiator, the equilibrium constant of the atom transfer reaction, and the propagation rate constant are dramatically affected by temperature. Shown in Figure 10 and Figure 11 are the comparisons of two polymerizations carried out at 90 °C (experiment 5) and 80 °C (experiment 10), respectively. At the lower temperature, the polymerization is slower, as expected. Furthermore, due to the slower rate of radical generation, the rate of radical termination is largely reduced. The initiation efficiency is thus expected to increase. On the other hand, the duration of the initiation process is extended, which increases the polydispersity, especially at low

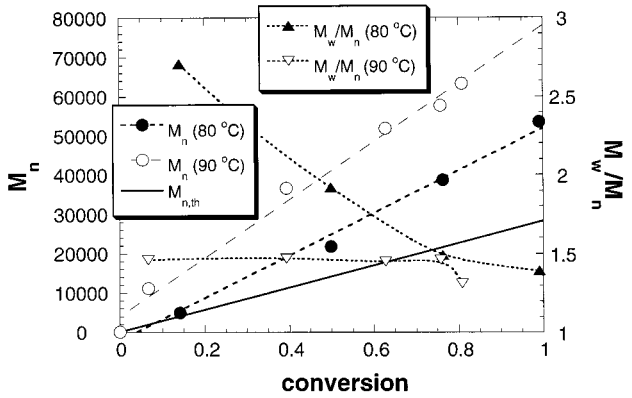

Figure 11. Temperature effect on the molecular weight evolution (see Table 4 for experimental conditions).

Table 7. Partitioning of Brij 98 between BMA and Water; BMA/Water = 15/100 (w/w)

	5% Brij 98		13.5% Brij 98	
	25 °C	90 °C	25 °C	90 °C
% in aq	96%	4%	97%	19%
$[\text{Brij 98}]_{aq}$	7.1 g/1L H_2O 6.2 mM	0.28 g/1L H_2O 0.24 mM	19.3 g/1L H_2O 16.8 mM	3.8 g/1L H_2O 3.4 mM

conversion. This is seen clearly in the molecular weight evolution plot.

From the colloidal stability point of view, the temperature also plays an important role in systems using a nonionic surfactant as the sole emulsifier. One of the major effects is a change in the phase behavior of the surfactant and hence the polymerization kinetics and the latex stability.[53] The influence of temperature is discussed further in the surfactant partitioning studies section.

Partitioning of the Surfactant. Compared with a conventional emulsion polymerization using an anionic surfactant, an unusually large amount of nonionic surfactant was employed under our experimental conditions in order to achieve a stable latex. However, not all surfactant molecules are present in the aqueous phase initially. This is indicated by the partitioning behavior of Brij 98 between BMA and water, which depends strongly on temperature, as shown in Table 7.

At room temperature, 95% of the surfactant is in the aqueous phase, regardless of the total amount of the surfactant. In contrast, at 90 °C decreased hydration of the hydrophilic moiety of the surfactant molecules makes the surfactant much more lipophilic. As a result, most of the surfactant is dissolved in the organic phase, and the concentration of the surfactant in the aqueous phase is strongly reduced. This explains the larger particle size and hence the less stable latex at 90 °C (189 ± 5 nm, Table 6) than at 80 °C (140 nm at 99% conversion) under otherwise identical conditions. Nevertheless, such low surfactant concentrations in water are still well above the cmc of Brij 98, which is 6×10^{-6} M at room temperature. This cmc value is expected to decrease at higher temperatures and is not very sensitive to the presence of $CuBr_2$ in the aqueous phase (Figure 12). Therefore, although organic partitioning of the surfactant is favored at the polymerization temperature, the initial emulsion is still rich in micelles.

Comparison between Reverse ATRP, Conventional Emulsion, and Miniemulsion Polymerizations. On the basis of the above results, the reverse

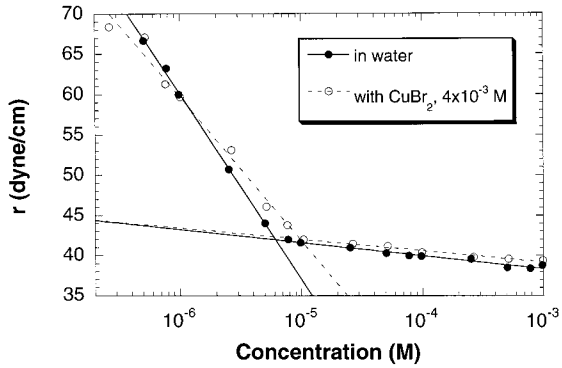

Figure 12. Cmc of Brij 98 at room temperature determined from surface tension measurement.

ATRP in the aqueous dispersed media provides an appealing system for comparison with the classical emulsion and miniemulsion systems, from which stable latexes with submicronic particles are produced. The initial state of a typical reverse ATRP is a monomer in water emulsion, determined by the dye solubility and the phase dilution method.[54] The water phase is saturated with monomer and contains the V-50 initiator, micelles swollen by monomer (partitioning and cmc studies of Brij 98), free molecules of surfactant, $CuBr_2$, and a small amount of the $CuBr_2$/dNbpy complex. Droplets are stabilized by the surfactant and contain the $CuBr_2$/dNbpy complex, the excess of free dNbpy, and the dissolved surfactant. The average size of the monomer droplets is much bigger than that of the micelles, as evidenced by the large average particle diameters (above micron) and excessive coagulum observed in the polymerization when an oil-soluble initiator such as AIBN was used.[55] Therefore, strong agitation is necessary to maintain the stability of the initial emulsion. The large monomer droplets, the presence of micelles, and the absence of cosurfactant clearly differentiate the reverse ATRP system from the classical miniemulsion polymerization.

When heat is applied, the decomposition of the initiator takes place in the water phase.

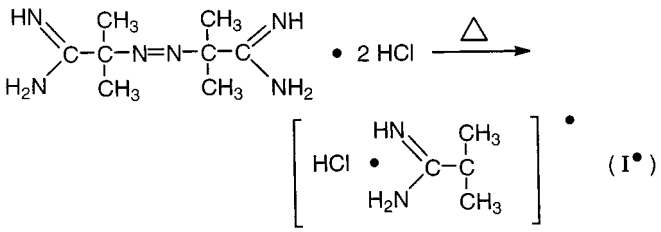

The formed primary radicals (I•) are then involved in the following possible steps:

(1) Initiation and propagation in the aqueous phase to form oligoradicals with the initiator fragment at the α-end. This reaction is relatively slow because of the low solubility of *n*-BMA in water (saturated concentration of *n*-BMA in water at 50 °C is 2.5×10^{-3} M).[8]

$$\text{I}^\bullet + n\text{BMA(M)} \rightarrow \text{I}-(\text{M})_n^\bullet$$

(2) Irreversible radical termination in the aqueous phase (which concerns the primary radicals, i.e., n or $m = 0$, as well as the oligoradicals).

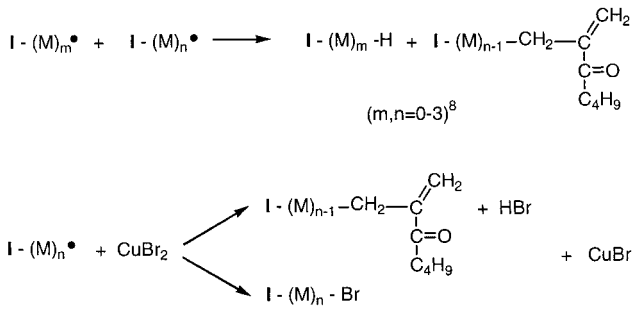

The termination between radicals is shown as a disproportionation reaction, but radical coupling is also possible. Two reactions between radicals and $CuBr_2$ may occur in the aqueous phase. The first one is β-hydrogen abstraction from the radical, the product of which is unable to initiate the polymerization;[56] the second one is the halogen transfer from $CuBr_2$ to the radical.[57,58] If the resulting bromine-ended oligomer is sufficiently surface active, it can enter the organic phase and act as the initiator in ATRP. However, if the alkyl bromide compound is not hydrophobic enough, it may stay in the aqueous phase and have little opportunity to be reactivated again. This is mainly because of the very low concentration of CuBr and dNbpy in the aqueous phase. In addition, the hydrolysis of the end group at elevated temperatures is also possible.

The above termination reactions in the aqueous phase may explain the low initiation efficiency generally observed for reverse ATRP. Furthermore, since the initiation efficiency is basically independent of the amount of the catalyst, as we have seen earlier, the termination between two radicals rather than between the radical and $CuBr_2$ seems to dominate.

As long as the oligoradicals are not irreversibly terminated, they grow by propagating in the water phase. Some of them reach a sufficient degree of polymerization to be surface-active or water-insoluble. Once the radicals enter the organic phase, instead of rapid propagation, they are transformed into the corresponding halide-terminated oligomers by deactivation, and $CuBr_2$/dNbpy is reduced to CuBr/dNbpy. This is the first major difference between classical polymerization and reverse ATRP in emulsion. The observed half-an-hour induction period is the result of this deactivation reaction in the organic phase. Considering the initiation efficiency and the partitioning of the Cu^{II} species in the organic phase, initially there is not enough Cu^{II} in the organic phase to trap all the oligoradicals coming from the aqueous phase. Taking experiment 1 as an example, the total amount of radicals entering the organic phase (i.e., the "living" chains which are formed in the particles) is 3.9×10^{-5} mol, while the initial Cu^{II} in the organic phase is about 1.5×10^{-5} mol after the partitioning. The fact that the polymerization is still "living" suggests that the $CuBr_2$ initially dissolved in the water phase must be able to quickly reenter the particles, form a complex with free dNbpy during the induction period, and supply the organic Cu^{II} consumed by the deactivation reaction. As long as the balance between Cu^{II} and Cu^{I} is not in favor of Cu^{I}, the polymerization rate remains very slow. The duration of the induction period depends on the ratio of $CuBr_2$/2dNbpy to the initiator (Figure 5), the concentration of the initiator (Figure 8), and the temperature (Figure 10). The last factor affects the decomposition rate of the initiator and the initiation

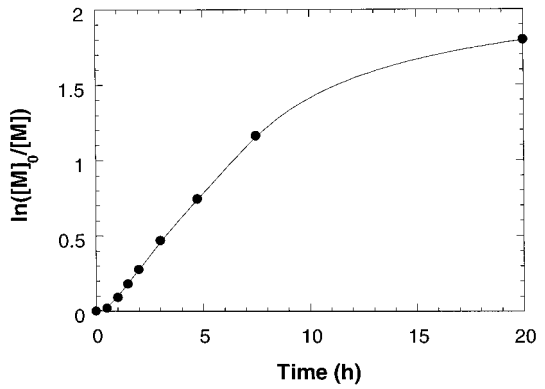

Figure 13. First-order kinetic plot for typical reverse ATRP in aqueous dispersed system. *n*-BMA/V-50/$CuBr_2$/dNbpy = 400/1/1.5/3, 90 °C. *n*-BMA/water = 1.5/10 (w/w), 13.5 wt % of Brij 98 vs monomer (experiment 1 in Table 4).

efficiency, the equilibrium constant of the atom transfer reaction, and the partitioning behavior of the catalyst and the surfactant. The half-life time of V-50 at 90 °C is estimated to be about 7−10 min ($k_d \approx (1.2-1.6) \times 10^{-3}$ s^{-1} with $E_a \approx 120-130$ kJ).[59] In other words, 90% of the initiator is consumed within half an hour.

When most of the radicals and Cu^{II} complex have been converted to the alkyl halides and the Cu^{I} complex, respectively, the polymerization rate starts to increase, and the induction period is over. In contrast to a conventional emulsion polymerization, there is little generation of radicals in the water phase since the majority of the initiator has been consumed. Actually, a high reaction temperature is used intentionally to avoid the continuous initiation that broadens the molar mass distribution of the polymers. At this stage, the propagating species are generated only via the activation step, and every particle behaves as an individual reactor. Hence, the kinetics of reverse ATRP is controlled entirely by the atom transfer equilibrium inside the polymer particles. The average number of radicals per particle ($\tilde{n}$) can be calculated according to the following equation:

$$\tilde{n} = N_A V_p [P^\bullet] = \frac{N_A \pi {D_p}^3 R_p}{6 k_p M_p} [M]_0$$

where N_A is Avogadro's number, V_p particle volume (dm^3), D_p swollen particle diameter (dm), R_p polymerization rate (s^{-1}), k_p the propagation constant (L mol^{-1} s^{-1}), M_p the monomer concentration in particle (mol/L), and $[M]_0$ the initial monomer concentration in the organic phase (mol/L).

The precise calculation, however, requires accurate measurement of each value at a given conversion and is thus beyond the scope of this study. Therefore, we attempted to estimate $\tilde{n}$ using a modified equation:

$$\tilde{n} = N_A V_p [P^\bullet] = \frac{N_A \pi {D_p}^3 \mathrm{SLOPE}}{6 k_p}$$

The SLOPE in the equation represents the slope (s^{-1}) of the first-order kinetic plot of the polymerization, as shown in Figure 13. It is uncommon to use the semilogarithmic plot in a heterogeneous system where free monomer droplets are present after the nucleation period, since the monomer concentration inside the particle stays constant before the free monomer droplets

disappear. Nevertheless, if the monomer droplets disappear at a relatively low conversion, the majority of the polymerization should display first-order kinetics, assuming the number of particles in the system is constant. (This assumption most likely holds due to the lack of radical supply from the aqueous phase.) From Figure 13, linearity is indeed observed within a large range of conversion (10−70%). The SLOPE is calculated as 4.6×10^{-5} s^{-1}. A rough estimation of $\tilde{n}$ in experiment 1 ($D_p = 200$ nm, $k_p = 2000$ L mol^{-1} s^{-1} [60]) gives a value of 0.06. This low value of $\tilde{n}$ means that the dominant event inside the particles is the reversible deactivation of the generated radical, which is responsible for the "living" character of the polymerization. At the same time, the irreversible termination continuously occurs. This process is even more pronounced than in the homogeneous organic medium, because in order to reach the same amount of the deactivator predicted by the persistent radical effect,[61,62] it is necessary to terminate more chains due to the partitioning of Cu^{II} species. This will eventually lead to a decreased $\tilde{n}$ with conversion, clearly shown by the curvature at high conversion in Figure 13.

The small value of $\tilde{n}$, plus the relatively large particle diameter (D_p > 180 nm), also explains why the polymerization rate is insensitive to the variation in the particle size within 40−50 nm (Figure 5). Indeed, a theoretical simulation points out that when the particle size is sufficiently large and the deactivator concentration high enough, the polymerization rate of a controlled radical polymerization based on a reversible termination mechanism in a dispersed medium should be little affected by the particle size.[63] The exclusive role of the surfactant is therefore to stabilize the formed particles.

Another important mechanistic difference between reverse ATRP and conventional emulsion polymerizations can be highlighted. It concerns the nucleation step. Owing to the deactivation process, at the end of the induction period when conversion starts to increase, the majority of the chains are created. But from a structural standpoint, they are reversibly or irreversibly terminated oligomers with very low molecular weight. Having a cationic charge at the α-end (from the initiator), these oligomers play the role of additional surfactant and have the freedom of moving from one site to another. Therefore, a conventional irreversible nucleation step, which would lead to the formation of small nuclei (precursor particle) able to grow by limited coagulation and consumption of monomer, does not take place. In contrast, the early stage of the system probably features the redistribution of the oligomers between the particles and possibly some small monomer droplets. Once a certain degree of polymerization is reached, the mobility of the polymer chains is lost, indicating the end of the "nucleation" period. Therefore, particle size and particle size distributions are closely related to the rate of polymerization during the early stage.

We have attempted to follow the particle growth with respect to the monomer conversion by measuring the particle size with light scattering. The measured diameter progressively decreases until 20% to 40% conversion and then stays nearly constant after 40% conversion (Figure 14, experiment 5).

Similar phenomena were observed regardless of the variation of experimental conditions, even in the absence of $CuBr_2$ and/or dNbpy (experiments 2−4). The latter experiments were regarded as the "conventional" emulsion polymerization. This particle evolution pattern may arise from using large amount of surfactant at elevated temperature or may be due to the interference in the measurements from the free monomer droplets (low conversion), as well as the remaining monomer inside the particles (after 40% conversion, monomer swollen particle). To study the nucleation mechanism, other techniques such as capillary hydrodynamic fractionation (CHDF) and transmission electronic microscopy (TEM) may provide more reliable information on the particle size and particle size distribution. A more precise kinetic study at the very low conversion is also necessary. Both gravimetry and gas chromotography that are used in the current study suffer from the sampling problem and may not generate kinetic data with sufficient accuracy.

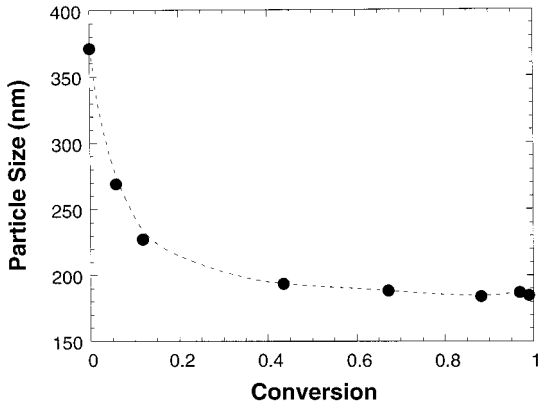

Figure 14. Particle size evolution for reverse ATRP of *n*-BMA. *n*-BMA/initiator/$CuBr_2$/dNbpy = 400/1/1.0/2, 90 °C, BMA/water = 1.5/10 (w/w), 13.5 w% of Brij 98 vs monomer (experiment 5 in Table 4).

Conclusion

In this work, reverse ATRP of *n*-butyl methacrylate has been successfully carried out in an aqueous dispersed system, using a water-soluble initiator. To control the polymerization, a hydrophobic ligand, dNbpy, was employed together with $CuBr_2$ to form the deactivator (and the activator CuBr/dNbpy complex in situ) for the atom transfer reaction. Although the partitioning study of the copper complexes indicates that not all the copper species are restricted to the organic phase, the linear correlation between the molecular weight and the monomer conversion as well as the narrow molar mass distributions confirms that the polymerization is still quite well controlled. The initiator efficiency is relatively low mainly due to the irreversible radical termination in the aqueous phase. Therefore, it is affected by the temperature and the initial concentration of the initiator but independent of the concentration of the catalyst and the surfactant. The particle size of the latex is between 150 and 300 nm and is a function of all the experimental variables investigated in this study, i.e., the temperature, the concentrations of the copper complex, the surfactant, and the initiator.

Brij 98, the nonionic surfactant used in this study, has a significant solubility in the organic phase under the polymerization conditions. But micelles are still present in large quantity in the initial emulsion. Because of the lack of high molecular weight polymer at the early polymerization stage, reverse ATRP in the aqueous dispersed system presumably has a very different "nucleation" mechanism from that of conventional

emulsion polymerization. In addition, the fast decomposition of the initiator avoids the continuous radical entry to the particles from the aqueous phase. As a result, the kinetics of the reverse ATRP is fundamentally different from a classical emulsion polymerization and is controlled mainly by the atom transfer equilibrium.

Acknowledgment. We are thankful to the CPS laboratory of CMU chemical engineering department for providing the particle sizing facility. The financial support from the ATRP Consortium at CMU and the US Environmental Protection Agency is greatly appreciated. We also thank Dr. Jianhui Xia for helpful discussions.

References and Notes

(1) Szwarc, M. *Nature* **1956**, *178*, 1168−1169.
(2) *Anionic Polymerization*: *Principles and Practical Applications*; Hsieh, H. L., Quirk, R. P., Eds.; Marcel Dekker: New York, 1996.
(3) *Cationic Polymerization*: *Mechanism, Synthesis and Applications*; Matyjaszewski, K., Ed.; Marcel Dekker: New York, 1996.
(4) Sogah, D. Y.; Webster, O. W. *Macromolecules* **1986**, *19*, 1775−1777.
(5) *Controlled Radical Polymerization*; ACS Symposium Series Vol. 685; Matyjaszewski, K., Ed.; American Chemical Society: Washington, DC, 1998.
(6) *Controlled/Living Radical Polymerization*: *Progress in ATRP, NMP, and RAFT*; ACS Symposium Series Vol. 768; Matyjaszewski, K., Ed.; American Chemical Society: Washington, DC, 2000.
(7) Odian, G. *Principles of Polymerization*, 3rd ed.; John Wiley & Sons: New York, 1991.
(8) Gilbert, R. G. *Emulsion Polymerization. A Mechanistic Approach*; Academic Press: London, 1995.
(9) *Emulsion Polymerization and Emulsion Polymers*; Lovell, P. A., El-Aasser, M. S., Eds.; John Wiley and Sons: Chichester, 1997.
(10) Solomon, D. H.; Rizzardo, E.; Cacioli, P. U.S. Patent 4,581,429, 1985.
(11) Georges, M. K.; Veregin, R. P. N.; Kazmaier, P. M.; Hamer, G. K. *Macromolecules* **1993**, *26*, 2987−2988.
(12) Benoit, D.; Grimaldi, S.; Finet, J. P.; Tordo, P.; Fontanille, M.; Gnanou, Y. *ACS Symp. Ser.* **1998**, *685*, 225−235.
(13) Benoit, D.; Chaplinski, V.; Braslau, R.; Hawker, C. J. *J. Am. Chem. Soc.* **1999**, *121*, 3904−3920.
(14) Kato, M.; Kmigaito, M.; Sawamoto, M.; Higashimura, T. *Macromolecules* **1995**, *28*, 1721−1723.
(15) Wang, J. S.; Matyjaszewski, K. *J. Am. Chem. Soc.* **1995**, *117*, 5614−5615.
(16) Matyjaszewski, K. *Chem. Eur. J.* **1999**, *5*, 3095−3102.
(17) Patten, T. E.; Matyjaszewski, K. *Adv. Mater.* **1998**, *10*, 901−915.
(18) Patten, T.; Matyjaszewski, K. *Acc. Chem. Res.* **1999**, *32*, 895−903.
(19) Chiefari, J.; Chong, Y. K.; Ercole, F.; Krstina, J.; Jeffery, J.; Le, T. P. T.; Mayadunne, R. T. A.; Meijs, G. G.; Moad, C. L.; Moad, G.; Rizzardo, E.; Thang, S. H. *Macromolecules* **1998**, *31*, 5559−5562.
(20) Charmot, D.; Corpart, P.; Adam, H.; Zard, S. Z.; Biadatti, T.; Bouhadir, G. *Macromol. Symp.* **2000**, *150*, 23−32.
(21) Matyjaszewski, K.; Gaynor, S. G.; Wang, J. S. *Macromolecules* **1995**, *28*, 2093−2095.
(22) Gaynor, S. G.; Wang, J. S.; Matyjaszewski, K. *Macromolecules* **1995**, *28*, 8051−8506.
(23) Bon, S. A. F.; Bosveld, M.; Klumperman, B.; German, A. L. *Macromolecules* **1997**, *30*, 324−326.
(24) Marestin, C.; Noel, C.; Guyot, A.; Claverie, J. *Macromolecules* **1998**, *31*, 4041−4044.
(25) Prodpran, R.; Dimonie, V. L.; Sudol, E. D.; El-Aasser, M. S. *Polym. Mater. Sci. Eng.* **1999**, *80*, 534−535.
(26) Lansalot, M.; Charleux, B.; Vairon, J.-P. *Am. Chem. Soc., Polym. Prepr.* **1999**, *40* (2), 317−318.
(27) Lansalot, M.; Farcet, C.; Charleux, B.; Vairon, J.-P.; Pirri, R.; Tordo, P. *ACS Symp. Ser.* **2000**, *768*, 138−151.
(28) Kanagasabapathy, S.; Claverie, J.; Uzulina, I. *Am. Chem. Soc., Polym. Prepr.* **1999**, *40* (*2*), 1080−1081.
(29) Uzulina, I.; Kanagasabapathy, S.; Claverie, J. *Macromol. Symp.* **2000**, *150*, 33−38.
(30) Lansalot, M.; Farcet, C.; Charleux, B.; Vairon, J.-P. *Macromolecules* **1999**, *32*, 7354−7360.
(31) Farcet, C.; Lansalot, M.; Pirri, R.; Vairon, J. P.; Charleux, B. *Macromol. Rapid Commun.* **2000**, in press.
(32) Butte, A.; Storti, G.; Morbidelli, M. *Macromolecules* **2000**, *33*, 3485−3487.
(33) Nishikawa, T.; Kamigaito, M.; Sawamoto, M. *Macromolecules* **1999**, *32*, 2204−2209.
(34) Lecomte, P.; Drapier, I.; Dubois, P.; Teyssie, P.; Jerome, R. *Macromolecules* **1997**, *30*, 7631−7633.
(35) Makino, T.; Tokunaga, E.; Hogen-Esch, T. E. *Am. Chem. Soc., Polym. Prepr.* **1998**, *39* (1), 288−289.
(36) Gaynor, S. G.; Qiu, J.; Matyjaszewski, K. *Macromolecules* **1998**, *31*, 5951−5954.
(37) Matyjaszewski, K.; Shipp, D.; Qiu, J.; Gaynor, S. G. *Macromolecules* **2000**, *33*, 2296−2298.
(38) Wan, X.; Ying, S. *J. Appl. Polym. Sci.* **2000**, *75*, 802−807.
(39) Chambard, G.; Man, P. D.; Klumperman, B. *Macromol. Symp.* **2000**, *150*, 45−51.
(40) Qiu, J.; Shipp, D.; Gaynor, S. G.; Matyjaszewski, K. *Am. Chem. Soc., Polym. Prepr.* **1999**, *40* (*2*), 418−419.
(41) Qiu, J.; Gaynor, S. G.; Matyjaszewski, K. *Macromolecules* **1999**, *32*, 2872−2875.
(42) Matyjaszewski, K.; Patten, T. E.; Xia, J. *J. Am. Chem. Soc.* **1997**, *119*, 674−680.
(43) Carter, S.; Megson, N. *J. Chem. Soc.* **1928**, 2954−2967.
(44) Doehlemann, E.; Fromherz, H. Z. *Z. Phys. Chem.* (*Munich*) **1934**, *A171*, 353.
(45) Barnes, J. C. *Inorg. Chem.* **1963**, *2*, 444−448.
(46) Qiu, J.; Pintauer, T.; Gaynor, S. G.; Matyjaszewski, K. *Am. Chem. Soc., Polym. Prepr.* **1999**, *40* (*2*), 420−421.
(47) *Handbook of Chemistry and Physics*, 79th ed.; Lide, D. R., Ed.; CRC Press: Boca Raton, FL, 1998−1999.
(48) Golub, G.; Lashaz, A.; Cohen, H.; Paoletti, P.; Benani, A.; Baltancoli, B. *Inorg. Chim. Acta* **1997**, *255*, 111.
(49) *Comprehensive Coordination Chemistry. The Synthesis, Reactions, Properties & Applications of Coordination Compounds*; Wilkinson, G., Gillard, R. D., McCleverty, J. A., Eds.; Pergamon Press: New York, 1987; Vol. 5, p 533.
(50) Conditions for homogeneous reverse ATRP: initiator: AIBN, *n*-BMA/AIBN/$CuBr_2$/dNbpy =400/1/1.5/3, 90 °C, polymerization carried out in sealed tubes, hexadecane as the GC internal standard.
(51) Moad, G.; Solomon, D. H. *The Chemistry of Free Radical Polymerization*; Elsevier Science Ltd.: New York, 1995.
(52) Jousset, S.; Qiu, J.; Matyjaszewski, K.; Granel, C. *Macromolecules*, to be submitted.
(53) Schomacker, R.; Muller, P. *DECHEMA Monogr.* **1995**, *131*, 75−85.
(54) Shinoda, K.; Friberg, S. *Emulsions and Solubilization*; Wiley: New York, 1986.
(55) Matyjaszewski, K.; Qiu, J.; Tsarevsky, N.; Charleux, B. *J. Polym. Sci., Polym. Chem. Ed.*, in press.
(56) Freiberg, M.; Meyerstein, D. *J. Chem. Soc., Faraday Trans. 1* **1980**, *76*, 1825−1837.
(57) Jenkins, C. L.; Kochi, J. K. *J. Am. Chem. Soc.* **1972**, *94*, 856−865.
(58) Jenkins, C. L.; Kochi, J. K. *J. Am. Chem. Soc.* **1972**, *94*, 843−855.
(59) Estimated based on $t_{1/2}$ = 10 h at 56 °C.
(60) *Polymer Handbook*, 4th ed.; Brandrup, J., Immergut, E. H., Grulke, E. A., Eds.; Wiley Publication: New York, 1999.
(61) Fischer, H. *Macromolecules* **1997**, *30*, 5666−5672.
(62) Fischer, H. *J. Polym. Sci., Part A*: *Polym. Chem.* **1999**, *37*, 1885−1901.
(63) Charleux, B. *Macromolecules* **2000**, *33*, 5358−5365.

MA000720Q